Stable isotope constraints on Holocene carbon cycle changes from an Antarctic ice core

Joachim Elsig[1], Jochen Schmitt[1,2], Daiana Leuenberger[1], Robert Schneider[1], Marc Eyer[1], Markus Leuenberger[1], Fortunat Joos[1], Hubertus Fischer[1,2] & Thomas F. Stocker[1]

[1]Climate and Environmental Physics, Physics Institute, University of Bern, Sidlerstrasse 5, CH-3012 Bern, Switzerland, and Oeschger Centre for Climate Change Research, University of Bern, Switzerland.
[2]Alfred Wegener Institute for Polar and Marine Research (AWI), Columbusstrasse, D-27568 Bremerhaven, Germany

Reconstructions of atmospheric CO_2 based on Antarctic ice cores[1, 2] reveal significant concentration changes during the Holocene, but the processes responsible for these CO_2 changes have not been unambiguously identified. Distinct characteristics in the carbon isotope signatures of the major carbon reservoirs (ocean, biosphere, sediments, and atmosphere) constrain variations in the CO_2 fluxes between those reservoirs. Here, we present the first highly resolved atmospheric $\delta^{13}C$ record for the last 11 kyr measured on atmospheric CO_2 trapped in an Antarctic ice core. Based on mass-balance inverse model calculations[3, 4] performed with a simplified carbon cycle model, we show that the decrease in atmospheric CO_2 of about 5 ppmv and the increase in $\delta^{13}C$ of about 0.25‰ during the early Holocene is most probably the result of a combination of carbon uptake of about 290 GtC by the land biosphere and carbon release from the ocean in response to carbonate compensation of the terrestrial uptake during the termination of the last ice age. The 20 ppmv increase of atmospheric CO_2 and the small decrease in $\delta^{13}C$ of about 0.05‰ during the later Holocene are dominated by contributions from carbonate compensation of earlier land biosphere uptake and coral reef formation, but only by a small decrease of the land biosphere carbon inventory.

The Holocene is the current interglacial period and started about 11 kyr BP (11,000 years before present, where present is defined as AD 1950) following the Transition (here defined as 18-11 kyr BP) from the last glacial maximum (LGM). Variations in the atmospheric concentration of CO_2 during the Holocene were significant but small compared to glacial-interglacial changes of typically 100 ppmv (parts per million by volume)[5, 6]. Yet, a decrease of about 5 ppmv from 11-7.5 kyr BP could be observed followed by an increase of about 20 ppmv to the pre-industrial level of about 280 ppmv[1, 2, 7]. Different explanations for these variations were discussed[7, 8] such as changes in the carbon inventories of vegetation, soils and peatlands[9], in anthropogenic land use[10, 11], in sea surface temperature[7, 12], coral reef growth[13, 14] or carbonate compensation[15]. The latter is a multi-millennial equilibration process of the atmosphere-ocean-sediment system and the weathering cycle. Moreover, model simulations of atmospheric CO_2 and $\delta^{13}C$ during the Holocene did not provide an unambiguous quantitative explanation[7, 8, 16]. The major stumbling block has been the scarcity of reconstructions of $\delta^{13}C$ on atmospheric CO_2 with sufficient accuracy and time resolution from the LGM to the Holocene[7, 17-20].

We performed carbon isotope measurements on air trapped in the EPICA (European Project for Ice Coring in Antarctica) Dome C (75°06´S, 123°24´E) ice core using two

completely independent extraction methods (mechanical cracking and sublimation, see supplementary information). Altogether, 199 single samples have been measured from 59 different depths in the interval of 110 to 410 meters. This interval corresponds to a gas age range of 11-0.35 kyr BP[21]. The results are gravitationally corrected (see Supplementary Information) and are presented in Figure 1. Of the 165 samples which were extracted with a mechanical cracker, a minimum of two were taken at each depth. For the remaining 34 samples we used a sublimation technique, and they are either single measurements or replications of three adjacent ice samples. The overall precision for a single measurement is 0.07‰ for both methods. The results of the two different methods agree very well within their uncertainties. The record clearly shows a continuous increase in the $\delta^{13}C$ values during the first 5 kyr of the Holocene followed by only slightly decreasing values.

We focus on the evolution of the carbon isotopes on a time scale of a few thousand years. Therefore, a spline and its 1σ uncertainty bands have been calculated with a cut-off period of 5 kyr (Figure 2). In a Monte Carlo simulation, standard deviations smaller than 0.07‰ were increased to 0.07‰; those higher than 0.07‰, however, were retained. Measurements at one depth interval (open symbols at 2.5 kyr BP in Figure 1) led to exceptionally negative $\delta^{13}C$ values significantly outside the 2σ uncertainty range independently for both extraction methods. The reason for these outliers remains obscure but the very large scatter in neighbouring samples despite the low-pass filtering effect of the bubble-enclosure process rules out an atmospheric origin of these outliers (see Supplementary Information). Accordingly, these two outliers are not included in the calculation of the spline.

Two main features of the carbon isotope record can be recognized: first, an almost linear increase from -6.58‰ to -6.33‰ between 11-6 kyr BP, and second, a small decrease of 0.05‰ in the later Holocene after 6 kyr BP. In Figure 2 our data are compared with two published $\delta^{13}C$ records from the Taylor Dome[7] and Law Dome[22] ice cores. The relative timing of the Taylor Dome to Dome C gas age was adapted from Monnin et al.[1], who matched the CO_2 records of Dome C and Taylor Dome for the Holocene. The Taylor Dome data generally agree with our measurements except for 3 data points (out of 12) that have no overlap within the reported 1σ uncertainties of our record. Our data are entirely consistent with the Law Dome record covering the last 1,000 years providing a direct link to direct atmospheric measurements through the firn gas data from Law Dome[22].

We use our new, more precise and better resolved $\delta^{13}C$ record to quantify carbon fluxes with different isotopic signatures and to test various hypotheses of Holocene CO_2 variations. Previous mechanistic model studies[8, 14, 16, 23], ocean sediment analyses[15], coral reef reconstructions[24], and peatland data[9, 25] suggest that the Holocene CO_2 variations were caused by (i) land biosphere uptake, (ii) carbonate compensation of earlier land biosphere uptake, and/or (iii) the build-up of coral reefs made of calcium carbonate. In contrast, changes in sea surface temperature (SST)[12], ocean circulation and marine biological cycling, shifts in the proportion of C_3 to C_4 photosynthesis[8], or changes in volcanic outgassing are assumed to be of minor importance for the Holocene CO_2 and $\delta^{13}C$ evolution. In addition, a strong release of carbon over the last 7,000 years from anthropogenic land use changes has been previously proposed[10]. The multitude and the spatio-temporal variability of the processes influencing atmospheric CO_2 and $\delta^{13}C$ prevent a firm attribution of the measured changes to a single mechanism. However, the deconvolution of our new

record by mass balance inverse calculations[3, 4, 7] (see Supplementary Information) permits us to quantify atmosphere-ocean and atmosphere-land carbon fluxes for different hypotheses and to attribute the measured CO_2 and $\delta^{13}C$ changes to the most likely mechanisms.

Model calculations were performed with a cost-efficient impulse response representation of carbonate compensation and of the High-Latitude Exchange/Interior Diffusion-Advection ocean model coupled to a 4-box representation of vegetation and soils and a well mixed atmosphere. The substitute model yields results for atmospheric CO_2 and the redistribution of carbon and carbon isotopes between global reservoirs that are comparable to those of spatially resolved models. For instance for the main scenario of land carbon uptake discussed below, the substitute yields a late Holocene CO_2 rise of 15 ppmv compared to 12 ppmv obtained with the Bern3D dynamic ocean-sediment model.

First, a land-biosphere only scenario is assessed. Atmospheric CO_2 variations are assumed to be entirely driven by changes in the land biosphere (using a fractionation for photosynthesis of 18.7‰[3]) and the ocean-sediment system to react only passively. Solving the atmospheric CO_2 budget for the unknown terrestrial flux yields a land biosphere uptake of 75 GtC from 11-7 kyr BP and a release of 275 GtC thereafter[7]. More importantly, the simulated evolution of atmospheric $\delta^{13}C$ is not compatible with the $\delta^{13}C$ measurements (Figure 2). The release of isotopically depleted terrestrial carbon yields a modelled $\delta^{13}C$ decrease of 0.25‰ after 8 kyr BP, whereas our data show little change. Thus, suggestions that CO_2 emissions from anthropogenic land use change caused the late Holocene CO_2 rise[10] are quantitatively inconsistent with our $\delta^{13}C$ record, as well as with other evidence[8].

Other scenarios considering only one driving mechanism (changes in SST, the marine biological cycle, or the calcium carbonate cycle only), or the combination of marine biological changes and land biosphere changes, are also in conflict with the measured co-evolution of CO_2 and $\delta^{13}C$ and with other proxy evidence. For example, an unrealistically large global average SST increase of 2.5°C is required to explain the $\delta^{13}C$ increase of 0.25‰ from 11-6 kyr BP by SST changes only. A combination of SST and land biosphere changes (tested by deconvolving both atmospheric records simultaneously) implies a global average SST increase of about 1.5°C, which is in conflict with alkenone-based SST reconstructions (0.2 ± 0.2°C since 8 kyr BP[26]) and model calculations[12, 27]. This is different from earlier findings by Indermühle et al.[7] who applied the same modelling approach but had to rely on only very few $\delta^{13}C$ values. They suggested that changes in the land biosphere with a modest temperature increase, possibly in combination with changes in the marine calcium carbonate cycle are responsible for the Holocene CO_2 evolution. Our improved $\delta^{13}C$ record permits us now to exclude this land biosphere-global SST scenario.

Finally, we turn to the land biosphere-marine carbonate scenario which assumes that atmospheric variations are caused by changes in the land biosphere in combination with carbonate compensation and coral reef growth. Both marine carbonate processes are associated with small isotopic fractionations and cannot be distinguished by $\delta^{13}C$ data nor can they significantly influence atmospheric $\delta^{13}C$. Solving the two atmospheric budgets for CO_2 and $\delta^{13}C$ yields a land biosphere uptake of (290 ± 36) GtC (mean and ±1σ confidence interval from a Monte Carlo

analysis) during 11-5 kyr BP and a release of (36 ± 37) GtC thereafter (Figure 3a). Note that the substitute model represents global mean fluxes and is not able to capture the influence of spatial variations in carbon and isotopic exchange. Potential contributions from other processes such as volcanism, SST changes or changes in the marine biological cycle are neglected in the land biosphere-marine carbonate scenario.

Are these fluxes inferred from our mass balance calculation realistic and in agreement with proxy data, model results, and process understanding? The early Holocene land biosphere uptake of 290 GtC is compatible with an early Holocene uptake of 110 GtC simulated by the Lund-Potsdam-Jena Dynamic Vegetation model on non-peatland land in response to reconstructed ice-sheet retreat, climate, and CO_2 variations[8]. This requires an early Holocene increase in peat carbon by 180 GtC. Current inventories of peat carbon range from 270 to 455 GtC[9]. Radiocarbon dating suggests initiation of peat accumulation already during the Transition with a major expansion of peat area in the early Holocene[9], but also some peat accumulation in recent millennia[28]. A land biosphere release of ~40 GtC in the later Holocene may be explained by (i) a model-estimated release of 30 GtC due to the desertification of the Sahara[7], (ii) a modelled release of around 50 GtC from pre-1,500 anthropogenic land use change[11], and (iii) an implied peat carbon uptake of ~40 GtC. The implied Holocene peat carbon uptake of 220 GtC is somewhat lower than the published range for the current carbon inventory in peat carbon[9]. This might be explained by peat carbon uptake during the Transition. Alternatively, natural carbon release from land might have been larger than 30 GtC[23] implying also a higher uptake by peat.

In a next step the atmosphere-ocean component of our carbon cycle model was used in forward simulations to test mechanistic explanations of inferred ocean-driven CO_2 changes. First, we prescribe the atmosphere-land fluxes from the land biosphere-carbonate compensation scenario to separate the contribution from Holocene land biosphere changes. The atmospheric $\delta^{13}C$ record is matched by design. The Holocene land biosphere changes result in an initial decrease in atmospheric CO_2 of about 17 ppmv, much larger than measured in ice cores, and an increase of ~9 ppmv after 6.5 kyr BP (Figure 3b). The increase is attributed to carbonate compensation of the early Holocene land biosphere uptake (~6 ppmv) and to the (prescribed) land biosphere release of 50 GtC (~3 ppmv). Second, we consider that carbonate compensation caused by the land biosphere uptake during the Transition also contributed to the Holocene CO_2 rise. Land biosphere carbon inventory changes over the glacial-interglacial period have been estimated to be around 500 to more than 1,000 GtC[29], [30]. Here, the land biosphere inventory is prescribed to increase linearly by 700 GtC during the Transition. This yields a simulated early Holocene CO_2 decrease comparable to the ice core data and a late Holocene rise of ~15 ppmv, somewhat smaller than reconstructed (see Supplementary Information for additional sensitivity simulations).

The remaining ~5 ppmv in atmospheric CO_2 can be plausibly explained by coral reef growth. Coral reef formation changes the carbonate ion balance in sea water and increases atmospheric CO_2[13]. Vecsei and Berger[24] reconstructed a calcium carbonate accumulation by reefs of 260 GtC during the past 8 kyr. This implies a CO_2 rise by another ~8 ppmv[14], compatible with the ice core data and model results. However, our modeling results and the $\delta^{13}C$ record do not quantitatively support the

suggestion that coral reef growth caused a much larger CO_2 rise by 20 to 40 ppmv[14] during the late Holocene.

High-resolution and high-precision ice core data on atmospheric $\delta^{13}C$ are able to significantly constrain the possible pathways of the carbon cycle evolution in the past. Based on carbon cycle modeling our new $\delta^{13}C$ data show that the evolution of atmospheric CO_2 in the past 11 kyr is dominated by an early Holocene increase in land biosphere and changes in the marine calcium carbonate cycle. Based on our $\delta^{13}C$ record suggestions that CO_2 emissions from anthropogenic land use changes caused the later Holocene CO_2 rise[10] and prevented a new ice age are not tenable. The attribution of the CO_2 changes to specific changes in the marine carbonate cycle (including coral reef growth, carbonate compensation of land biosphere carbon uptake, sediment-ocean interactions related to the reorganization of the marine carbon cycle during the glacial-interglacial transition, or changes in weathering fluxes) is challenging. Further progress requires an extension of our atmospheric $\delta^{13}C$ record into the glacial period as well as process studies with 3-dimensional physical-biogeochemical climate models.

References

1. Monnin, E. et al. *Atmospheric CO_2 concentrations over the last glacial termination*. Science **291**, 112-114 (2001).
2. Flückiger, J. et al. *High-resolution Holocene N_2O ice core record and its relationship with CH_4 and CO_2*. Global Biogeochemical Cycles **16**, 10.1-10.8 (2002).
3. Joos, F. & Bruno, M. *Long-term variability of the terrestrial and oceanic carbon sinks and the budgets of the carbon isotopes ^{13}C and ^{14}C*. Global Biogeochemical Cycles **12**, 277-295 (1998).
4. Bruno, M. & Joos, F. *Terrestrial carbon storage during the past 200 years: A Monte Carlo analysis of CO_2 data from ice core and atmospheric measurements*. Global Biogeochemical Cycles **11**, 111-124 (1997).
5. Lüthi, D. et al. *High-resolution carbon dioxide concentration record 650,000-800,000 years before present*. Nature **453**, 379-382 (2008).
6. Sigman, D. M. & Boyle, E. A. *Glacial/interglacial variations in atmospheric carbon dioxide*. Nature **407**, 859-869 (2000).
7. Indermühle, A. et al. *Holocene carbon-cycle dynamics based on CO_2 trapped in ice at Taylor Dome, Antarctica*. Nature **398**, 121-126 (1999).
8. Joos, F., Gerber, S., Prentice, I. C., Otto-Bliesner, B. L. & Valdes, P. J. *Transient simulations of Holocene atmospheric carbon dioxide and terrestrial carbon since the Last Glacial Maximum*. Global Biogeochemical Cycles **18**, 1-18 (2004).
9. MacDonald, G. M. et al. *Rapid early development of circumarctic peatlands and atmospheric CH_4 and CO_2 variations*. Science **314**, 285-288 (2006).
10. Ruddiman, W. F. *The anthropogenic greenhouse era began thousands of years ago*. Climatic Change **61**, 261-293 (2003).
11. Strassmann, K. M., Joos, F. & Fischer, G. *Simulating effects of land use changes on carbon fluxes: past contributions to atmospheric CO_2 increases and future commitments due to losses of terrestrial sink capacity*. Tellus Series B-Chemical and Physical Meteorology **60**, 583-603 (2008).
12. Brovkin, V., Kim, J. H., Hofmann, M. & Schneider, R. *A lowering effect of reconstructed Holocene changes in sea surface temperatures on the atmospheric CO_2 concentration*. Global Biogeochemical Cycles **22**, GB1016 (2008).
13. Berger, W. H. *Increase of Carbon-Dioxide in the Atmosphere during Deglaciation - the Coral-Reef Hypothesis*. Naturwissenschaften **69**, 87-88 (1982).
14. Ridgwell, A. J., Watson, A. J., Maslin, M. A. & Kaplan, J. O. *Implications of coral reef buildup for the controls on atmospheric CO_2 since the Last Glacial Maximum*. Paleoceanography **18**, 1083-1092 (2003).
15. Broecker, W. S., Lynch-Stieglitz, J., Clark, E., Hajdas, I. & Bonani, G. *What caused the atmosphere's CO_2 content to rise during the last 8000 years?* Geochemistry Geophysics Geosystems **2**, art. no.-2001GC000177 (2001).
16. Brovkin, V. et al. *Carbon cycle, vegetation, and climate dynamics in the Holocene: Experiments with the CLIMBER-2 model*. Global Biogeochem. Cycles **16(4)**, (86-1)-(86-13) (2002).
17. Smith, H. J., Fischer, H., Wahlen, M., Mastroianni, D. & Deck, B. *Dual modes of the carbon cycle since the Last Glacial Maximum*. Nature **400**, 248-250 (1999).

18. Leuenberger, M., Siegenthaler, U. & Langway, C. C. *Carbon Isotope Composition of Atmospheric CO_2 during the Last Ice-Age from an Antarctic Ice Core*. Nature **357**, 488-490 (1992).
19. Eyer, M. *Highly resolved $\delta^{13}C$ measurements on CO_2 in air from Antarctic ice cores*. PhD Thesis, Climate and Environmental Physics, Physics Institute, University of Bern, 1-113 (2004).
20. Lourantou, A. *Contraindre l'augmentation en dioxyde de carbone (CO_2) lors des déglaciations basés sur son rapport isotopique stable du carbone ($\delta^{13}CO_2$)*. PhD Thèse de l'Université Joseph Fourier, Grenoble 1, France (2008).
21. Loulergue, L. et al. *New constraints on the gas age-ice age difference along the EPICA ice cores, 0-50 kyr*. Climate of the Past **3**, 527-540 (2007).
22. Francey, R. J. et al. *A 1000-year high precision record of $\delta^{13}C$ in atmospheric CO_2*. Tellus Series B-Chemical and Physical Meteorology **51**, 170-193 (1999).
23. Schurgers, G. et al. *Dynamics of the terrestrial biosphere, climate and atmospheric CO_2 concentration during interglacials: a comparison between Eemian and Holocene*. Climate of the Past **2**, 205-220 (2006).
24. Vecsei, A. & Berger, W. H. *Increase of atmospheric CO_2 during deglaciation: Constraints on the coral reef hypothesis from patterns of deposition*. Global Biogeochemical Cycles **18**, GB1035 (1-7) (2004).
25. Smith, L. C. et al. *Siberian peatlands a net carbon sink and global methane source since the early Holocene*. Science **303**, 353-356 (2004).
26. Kim, J. H. et al. *North Pacific and North Atlantic sea-surface temperature variability during the holocene*. Quaternary Science Reviews **23**, 2141-2154 (2004).
27. Wang, Y., Mysak, L. A. & Roulet, N. T. *Holocene climate and carbon cycle dynamics: Experiments with the "green" McGill Paleoclimate Model*. Global Biogeochemical Cycles **19**, GB3022 (2005).
28. Beilman, D. W., MacDonald, G. M., Smith, L. C. & Reimer, P. J. *Carbon accumulation in peatlands of West Siberia over the last 2000 years*. Global Biogeochem. Cycles **23**, GB1012 (2009).
29. Duplessy, J. C. et al. *Deepwater source variations during the last climatic cycle and their impact on the global deepwater circulation*. Paleoceanography **3**, 343–360 (1988).
30. Crowley, T. J. *Ice-Age Terrestrial Carbon Changes Revisited*. Global Biogeochemical Cycles **9**, 377-389 (1995).

Supplementary Information is linked to the online version of the paper at www.nature.com/nature.

Acknowledgements This work is a contribution to the European Project for Ice Coring in Antarctica (EPICA), a joint European Science Foundation/European Commission scientific programme, funded by the EU (EPICA-MIS) and by national contributions from Belgium, Denmark, France, Germany, Italy, the Netherlands, Norway, Sweden, Switzerland and the United Kingdom. The main logistic support was provided by IPEV and PNRA (at Dome C) and AWI (at Dronning Maud Land). We thank A. Landais, D. Rodriguez, E. Capron and G. Dreyfus for the contribution of $\delta^{15}N$ data as well as P. Nyfeler and K. Grossenbacher for their technical support, T. Tschumi for sharing his Bern3D results, and J. Chappellaz for comments. We acknowledge financial support by the Swiss NSF, the DFG priority program INTERDYNAMIK and the German climate program DEKLIM. This is EPICA publication no. 227.

Author contribution J.E., J.S., D.L., R.S., and M.E. performed the measurements. F.J. performed modelling and interpretation. M.L., H.F., and T.F.S designed research. All authors participated in discussions on method development, interpretation and presentation of results.

Author information Reprints and permissions information is available at www.nature.com/reprints. Correspondence and requests for materials should be addressed to T.F.S. (stocker@climate.unibe.ch).

Figure legends

Figure 1

$\delta^{13}C$ and CO_2[1, 2] measured in air trapped in ice from Dome C, Antarctica. Blue triangles indicate measurements performed with the cracker (mean of two to four samples), red circles measurements with the sublimation method (single measurements or mean of three adjacent samples). Open symbols indicate outliers. The error bars represent the t-weighted 1σ standard deviations of the mean (s.d.m). Grey squares represent CO_2 data from Dome C (mean of six samples; error bars, 1σ of the mean)[21].

Figure 2

$\delta^{13}C$ ice core records measured on the Antarctic ice cores from Dome C, Taylor Dome[7] and Law Dome[22]. Grey, yellow, and green colored symbols refer to results from Dome C, Taylor Dome and Law Dome, respectively. Grey open symbols indicate outliers. The error bars for Dome C measurements are the same as in Fig. 1. The error bars for the Taylor Dome and Law Dome data represent 1σ of the mean (s.d.). The grey line through the Dome C data represents the mean of one hundred Monte Carlo simulations with a cut-off period of 5 kyr. The grey shaded area indicates the 1σ standard deviation of the spline (s.d.). The red line is the result of a deconvolution of the atmospheric CO_2 record assuming the land biosphere scenario.

Figure 3

Attribution of simulated CO_2 to different processes. (a) Cumulative land biosphere uptake for the land biosphere-marine carbonate scenario from deconvolving the atmospheric CO_2[1, 2] and $\delta^{13}C$ records. The shaded area indicates the 1σ confidence interval of a Monte Carlo analysis[4], taking into account the uncertainty of the ice-core data. (b) Atmospheric CO_2 is simulated by prescribing the land biosphere changes shown in (a). Grey squares represent CO_2 data from Dome C (mean of six samples; error bars, 1σ of the mean). Green line: land biosphere only; black line: land biosphere and carbonate compensation (carb. comp.) during the Holocene; red line: including 700 GtC land biosphere uptake during the Transition. The bar chart indicates the modelled contributions to the CO_2 rise from 6.5-0 kyr BP by individual processes assuming the land biosphere-marine carbonate scenario. The remaining difference between the simulated and measured CO_2 increase may be attributed to coral reef growth and other mechanisms.

Methods summary

For the cracker method we use a mechanic extraction device (steel needle cracker), which crushes the ice sample (6 g) under vacuum to release the enclosed gases in the ice. In case of the sublimation method the gases are extracted from the ice sample (30 g) using sublimation at -25°C in a glass vessel. In either case the released air is dried in a water trap and the amount of air is measured with a pressure gauge to calculate the CO_2 concentration. CO_2 and N_2O are separated from the major air components at -196°C using liquid nitrogen with subsequent concentration by means of a cryofocus capillary to ensure complete gas chromatographic separation. After having passed a chromatographic column to separate isobaric components (N_2O and organic components from drilling fluid) the purified CO_2 sample is injected via an open-split into the isotope ratio mass spectrometer (a Delta Plus XL for the cracker method and a MAT 253 for the sublimation method, both ThermoFisher). Both extraction systems are equipped with inlet devices which allow processing calibrated reference gases in the same way as ice samples. This allows checking the system and referencing the results from the ice samples on an international standard.

Figure 1

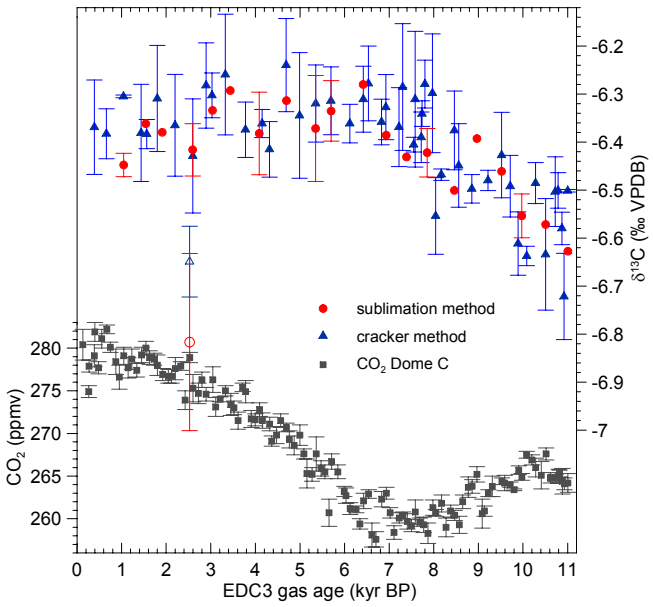

Stable isotope constraints on Holocene carbon cycle changes from an Antarctic ice core

Elsig et al.

Figure 2

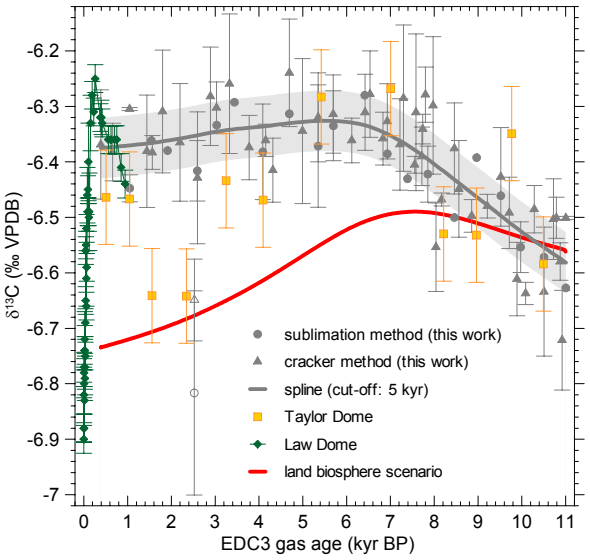

Stable isotope constraints on Holocene carbon cycle changes from an Antarctic ice core

Elsig et al.

Figure 3

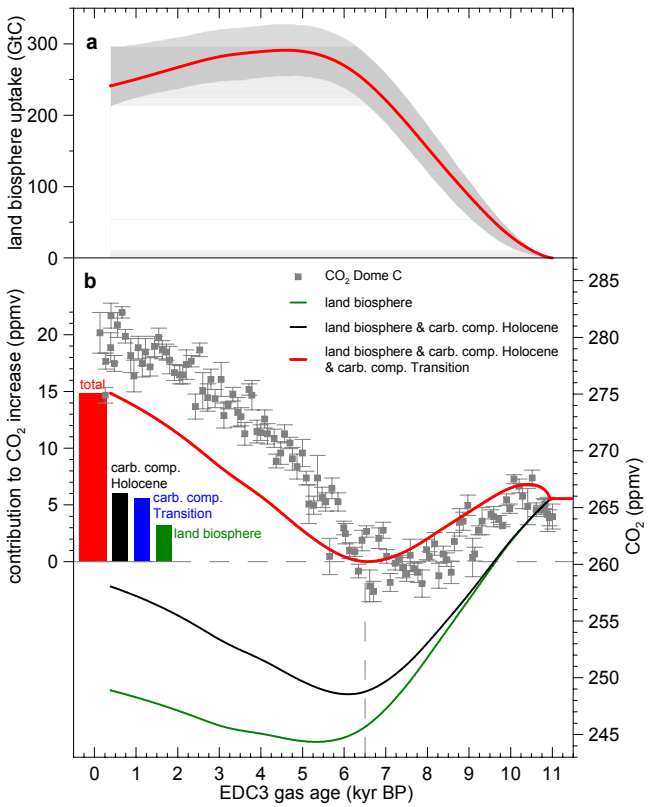

Stable isotope constraints on Holocene carbon cycle changes from an Antarctic ice core

Elsig et al.

Supplementary Information

to

Stable isotope constraints on Holocene carbon cycle changes from an Antarctic ice core

Joachim Elsig, Jochen Schmitt, Daiana Leuenberger, Robert Schneider, Marc Eyer, Markus Leuenberger, Fortunat Joos, Hubertus Fischer & Thomas F. Stocker

Cracker method:

One sample requires 5-6 g of ice ($V = l \cdot w \cdot h = 2.2 \cdot 1.5 \cdot 2.2$ cm^3). This corresponds to about 0.5 ml STP of air or 0.1 µl STP CO_2. A stainless steel needle cracker is lined up with the preconcentration system (Precon) and a Delta Plus XL mass spectrometer (MS) from ThermoFisher allowing online measurements. The ice cracker consists of a stainless steel body (57 ml) in which an array of stainless steel needles is mounted to crack the ice under vacuum at a temperature of -20°C. The released gas expands through a water trap (-70°C) into a small volume, where the gas pressure to evaluate the CO_2 concentration is measured. The extracted air is then flushed by a high helium flux of about 600 ml/min through the cracker to the Precon. This unit permits the quantitative separation of CO_2 and N_2O from air as well as switching from a high to a low helium stream (~1 ml/min). After having passed a GC (gas chromatography) column to separate CO_2 from N_2O and possible organic components, e.g. derived from drilling fluid, the CO_2 sample is injected into the MS via an open-split. During one day of measurements several runs with bubble free ice (EK) combined with a gas of known isotopic composition (EG II, $\delta^{13}C$ = -4.74‰ VPDB) are performed. These standard gas measurements allow checking the system and referencing the samples[1].

Sublimation method:

The retrieval of $\delta^{13}C$ values on CO_2 from gas enclosures in ice cores using sublimation (together with $\delta^{18}O$ and mixing ratios of CO_2 and N_2O) is split into two separate analytical systems: First, the gas extraction using sublimation in a vacuum line and secondly, a sample clean-up in a helium flow line coupled to continuous flow isotope ratio mass spectrometry (CF-IRMS).

The principle behind the gas extraction is sublimation allowing for a quantitative release of air trapped in either bubble or clathrate ice samples. Within a glass vessel, a cylindrical ice sample of 30 g is held at -25°C via a cold air stream. By illuminating the sample with infrared light a water vapour flux is established from the sample to a nearby cold trap thereby quantitatively releasing the enclosed gases. This gas stream is dried in a cold trap at -120°C and afterwards CO_2 and N_2O are separated from the major air components (N_2, O_2, Ar) at -196°C. The amount of the major air components is measured with a pressure gauge connected to a temperature controlled expansion volume. Together with the signal from the mass spectrometer

the mixing ratios of CO_2 and N_2O can be calculated by referencing it to the standard gas concentrations. CO_2 and N_2O are transferred into a glass tube, which is then flame-sealed to be stored until the clean-up and measurement step. The extraction line is equipped with a gas inlet to continuously inject calibrated air samples into the sublimation vessel, thus, mimicking the continuous gas release during the sublimation of an ice sample. These air samples are used as a reference for both the isotopic measurement and the mixing ratio of CO_2 and to monitor the entire analysis.
The sample clean-up line consists of a tube cracker device to open the sealed glass tubes within a helium flux of 0.9 ml min^{-1}, a cryofocus capillary to generate a sharp sample peak and a chromatographic column to separate isobaric components (N_2O and organic components from drilling fluid) from CO_2. Finally, pure CO_2 is then admitted to a Finnigan 253 IRMS (isotope ratio mass spectrometer) via an open split interface. This off-line set-up minimizes additional uncertainty introduced by the clean up and IRMS measurement procedure as all samples can be measured at the identical instrument conditions thus, day to day instrument variations are omitted. Like the gas extraction line, the sample clean-up line is equipped with a reference device to introduce working standards of CO_2/N_2O prior to each ice or air sample. The peak size of the working standard can be adjusted to cover the range of sample sizes thereby accounting for a potential dependency of the $\delta^{13}C$ signal on CO_2 amount[2].

Discussion of the outlier at 2.5 kyr BP

The samples with a gas age of 2,519 yr BP were not taken into account for the interpretation and for calculating splines. Air from this depth was extracted independently with the cracker as well with the sublimation method. Both methods indicate a much too negative $\delta^{13}C$ value. A closer look on the raw data of this depth interval revealed that replicate ice samples only a few cm apart (or a few years in age) show $\delta^{13}C$ variations of 0.4‰. Given the broad age distribution of the enclosed air (around 170 years) we can clearly rule out an atmospheric perturbation as cause. As the CO_2 concentration measured on the same samples deviate only by a few ppmv from neighbouring depth intervals a post drilling contamination with recent atmospheric air (with more negative $\delta^{13}C$ values and elevated CO_2 concentration) can be ruled out as well. However, just 0.3 m above this interval drilling problems occurred (E. Wolff, personal communications) likely generating extreme mechanic stress on the ice below which can be responsible for these outliers, yet the underlying process is not understood.

Gravitation correction:

As mentioned in the text, the isotopes of the enclosed air are fractionated due to gravitational settling. As a result, the heavy isotopes are concentrated at the bottom of the firn column. Accordingly, the enclosed air in the ice is enriched in heavy molecules. This fractionation depends on the mass difference of the gas species, the mean site temperature and on the diffusive column height of the firn. Since the isotopic composition of atmospheric N_2 remained constant over long time intervals, measuring $\delta^{15}N$ in air from ice cores can be used to correct $\delta^{13}C$ for the gravitation effect. Thereby, changes in $\delta^{15}N$ can directly be applied to correct $\delta^{13}C$ values since

the mass differences of the involved isotopes are the same. Existing $\delta^{15}N$ data for Dome C are shown in Figure S1 (b). The single $\delta^{15}N$ value at 0 yrs BP is taken from firn measurements performed within the framework of the EU project FIRETRACC[3]. $\delta^{15}N$ values from 1 to 9 kyr BP are unpublished values measured at LSCE in 2008 (D. Rodriguez, E. Capron and A. Landais, personal communication), and $\delta^{15}N$ values after 9 kyr BP were measured at LSCE[4] in 2003. Also shown in Figure S1 are two splines of our data set, one through the uncorrected data and the other through the gravitation corrected data. The influence of the gravitation correction is summarised in Table ST1:
The main difference is the time when the $\delta^{13}C$ maximum is reached (T_{max}). Since the gravitation correction is almost constant during the Holocene, the main conclusions are not affected by this correction. Therefore, the increase in $\delta^{13}C$ by about 0.25‰ in the early Holocene and the slight decrease in the late Holocene are robust.

Comparison of extraction methods (cracker and sublimation):
Since the measurements were performed with two different extraction methods and two distinct mass spectrometers and separate standard gases, the two data sets have to be checked for a possible offset. Therefore, splines were calculated for both records (Figure S2). Additionally, Table ST2 summarises the main features of the two records including a comparison between the slopes from 11-8 kyr BP and 6-0 kyr BP. The main differences between the two records are the point of time, T_{max}, where the maximum $\delta^{13}C$ value is reached as well as the strength of the decrease after this point. Both records suggest an increase of $\delta^{13}C$ between 11-8 kyr BP. Within the error of the slopes, this increase is robust. The decrease after 6 kyr BP is slightly higher for the sublimation measurements but it is also consistent within the measurements errors.

Comparison with a former $\delta^{13}C$ record derived with the cracker method
Another unpublished $\delta^{13}C$ record over the Holocene period was already established in 2004 with a cracker system similar to the one used in this study but with a significantly higher scatter[5]. A compilation of all three records is shown in Figure S3.
Within the range of error, the data derived earlier are in good agreement with the data presented in the main text except for the period from about 8 to 7 kyr. Here, the older measurements are systematically too low by about 0.4‰. So far we have not been able to find any explanation for this deviation. Since this early study, however, substantial progress has been made by constructing an improved and dedicated cracker system, and by including a gas chromatographic column which helped to significantly reduce the measuring uncertainty. Therefore, we refrain from including this data set into the discussion in the main text.

Splines for different cut-off periods:
In order to quantify the effect of different cut-off periods, splines[6] were calculated for cut-off periods between 0.5 kyr and 6 kyr (Figure S4). For periods between 0.5-1 kyr, the splines are not smooth but show millennial oscillations. Considering our

uncertainty of ±0.07‰, and the time resolution of our data, these oscillations are not significant and cannot be interpreted. However, it is noteworthy that the Law Dome ice core data[7] show a wiggle that would be in line with millennial oscillations suggested by our new Holocene record. Data with further improved precision and time resolution are needed to verify or falsify such millennial-scale oscillations. For a cut-off period of more than 3 kyr, the oscillations disappear and the long-term trend as mentioned in the text becomes visible.

Mass-spectrometric CO_2 measurements:

With both of our measuring set-ups it is possible to estimate the CO_2 concentration parallel to $\delta^{13}C$ values. The CO_2 concentration can be calculated by comparing the ratio of the gas extraction pressure and the peak area of mass to charge ratio 44 in the mass spectrometer with the corresponding ratio of a standard gas. The mean reproducibility for the cracker and sublimation methods is 2.6 ppmv and 2.9 ppmv, respectively. This is about twice as much as for the dedicated CO_2 concentration method[8]. Concerning the cracker measurements the main uncertainty lies in the behaviour of the water vapour and desorption/adsorption effects during the cracking process and the subsequent pressure measurement. Water vapour may account for a small pressure increase and possibly affects the pressure readings. In case of the concentration results from the sublimation method the pressure reading is sensitive to temperature fluctuations which may explain the larger scatter and slightly higher values. The results are presented in Figure S5 in comparison with the measurements performed on the EDC96 ice by a laser absorption spectroscopy method[9].

Model description and additional results

Model description

Model calculations were performed with an impulse response representation of the High-Latitude Exchange/Interior Diffusion-Advection (HILDA) ocean model coupled to a 4-box representation of vegetation and soils and a well-mixed atmosphere[10]. Carbonate compensation is included by assuming that a fraction, *a*, of 70% of the terrestrial release (uptake) is absorbed by sediments on an exponential timescale, τ, of 5 kyr[11, 12]. A $^{13}C/^{12}C$ fractionation of 18.7‰ is applied for the atmosphere-to-land biosphere flux and fractionation for fluxes between atmosphere and surface ocean are from Mook[13] as described elsewhere[14].

Mass-balance inverse model calculations

Carbon fluxes in the land biosphere-only scenario (S_1) are quantified by a (single) deconvolution of the atmospheric CO_2 record[15]. Atmospheric CO_2 is prescribed and carbon uptake by the ocean-sediment system is simulated. The total carbon inventory in the atmosphere-land biosphere-ocean-sediment system remains constant. Then, the net land biosphere-to-atmosphere flux is equal to the prescribed change in the atmospheric carbon inventory and the calculated ocean uptake flux. The land biosphere-global SST (SST: sea surface temperature) scenario (S_2), the land biosphere-marine biosphere scenario (S_3), and the land biosphere-marine carbonate compensation scenario (S_4) are quantified by (double) deconvolutions of

the atmospheric CO_2 and $\delta^{13}C$ records as detailed by Joos and Bruno[14] and Indermühle et al.[11]. In the land biosphere-global SST scenario, the partial pressure of CO_2 in the surface ocean is forced to be consistent with the inferred net sea-to-air flux (from the mass balance of CO_2 and $^{13}CO_2$) and the prescribed atmospheric CO_2 by adjusting global SST in the model. The isotopic fractionation for the air-sea and sea-air fluxes is evaluated for the adjusted global SST. In the land biosphere-marine biosphere scenario, the surface ocean CO_2 partial pressure is similarly adjusted by adding (removing) dissolved inorganic carbon that is depleted in $\delta^{13}C$ by 20‰ relative to the surface ocean ^{13}C to ^{12}C ratio. In the land biosphere-carbonate compensation scenario, the surface partial pressure is adjusted without modification of the ^{13}C to ^{12}C ratio. The small fractionation of ~1‰ that occurs during calcium carbonate formation is neglected.

The land biosphere-global SST scenario S_2 yields a net carbon flux of about 190 GtC to the terrestrial biosphere from 11-6 kyr BP and a decrease of the terrestrial biosphere of 120 GtC from 6-0 kyr BP (Figure S6). Derived global SST indicates an increase by about 1.5°C over the Holocene, which is unrealistic. The double deconvolution for the land biosphere-marine biosphere scenario S_3 leads to unrealistically high terrestrial carbon fluxes and requires an increase of the terrestrial biosphere of about 700 GtC from 11-3.5 kyr BP followed by a decrease of 100 GtC from 3.5-0 kyr BP. Such large fluxes and the large increase in the terrestrial biosphere during the Holocene are most unlikely and in contrast to vegetation model estimates[12] and pollen-based reconstructions of vegetation cover[16]. However, we can not entirely exclude that marine biological processes have contributed to the co-evolution of atmospheric CO_2 and $\delta^{13}C$.

Sensitivity of simulated CO_2 to the timescales of carbonate compensation and the temporal evolution terrestrial carbon uptake during the transition

Model simulations were performed to project atmospheric CO_2 from prescribed land biosphere-atmosphere fluxes to evaluate whether the results of the mass balance inverse calculation for the land biosphere-carbonate scenario are plausible. The sensitivity of simulated CO_2 to changes in the following parameters is addressed: carbonate compensation timescale τ; the fraction *a* of the perturbation to be mitigated by carbonate compensation, and the uptake history of the terrestrial biosphere. Four different schematic uptake histories prior to the Holocene are selected and shown in Figure S7: (i) no land biosphere uptake during the Transition to detect the effect of the carbonate compensation caused by the land biosphere uptake during the early Holocene; (ii), the standard uptake that assumes a linear increase in the land biosphere inventory of 700 GtC during the Transition in 7 kyr (constant flux of 0.1 GtC yr^{-1} from 18 to 11 ka BP); (iii), a rapid land biosphere uptake of 700 GtC in 2 kyr; and (iv), a slow land biosphere uptake of 700 GtC in 10 kyr. The CO_2 decrease in the early Holocene is stronger and the increase during the late Holocene is smaller for the 10 kyr uptake history compared to the standard. A rapid but intense uptake history during the Transition (iii) results in a stronger increase of CO_2 during the late Holocene. The measured atmospheric CO_2 data are simulated better when τ is set to 7 kyr and the fractionation *a* is increased to 0.8. Good agreement with the data in these still very simplified scenarios results for τ = 8 kyr, *a* = 0.8 and assuming a rapid and large land biosphere uptake during the period 13 to 11 kyr BP. This reflects a scenario with a small role of coral reef buildup for Holocene CO_2.

References:

1. Elsig, J. *New insights into the global carbon cycle from measurements of CO_2 stable isotopes: methodological improvements and interpretation of a new EPICA Dome C ice core $\delta^{13}C$ record*. PhD Thesis, Climate and Environmental Physics, Physics Institute, University of Bern, 1-174 (2009).
2. Schmitt, J. *A sublimation technique for high-precision $\delta^{13}C$ on CO_2 and CO_2 mixing ratio from air trappes in deep ice cores*. PhD Thesis, Fachbereich Geowissenschaften, Universität Bremen, 1-167 (2006).
3. FIRETRACC. in Part C: Scientific Report (European Commission DGX, Environment and Climate, 2000).
4. Dreyfus, G. *Dating an 800,000 year antarctic ice core record using the isotopic composition of trapped air*. PhD thesis, Departement of Geoscience, Princeton University (2008).
5. Eyer, M. *Highly resolved $\delta^{13}C$ measurements on CO_2 in air from Antarctic ice cores*. PhD Thesis, Climate and Environmental Physics, Physics Institute, University of Bern, 1-113 (2004).
6. Enting, I. G. *On the Use of Smoothing Splines to Filter CO_2 Data*. Journal of Geophysical Research-Atmospheres **92**, 10977-10984 (1987).
7. Francey, R. J. et al. *A 1000-year high precision record of $\delta^{13}C$ in atmospheric CO_2*. Tellus Series B-Chemical and Physical Meteorology **51**, 170-193 (1999).
8. Lüthi, D. et al. *High-resolution carbon dioxide concentration record 650,000-800,000 years before present*. Nature **453**, 379-382 (2008).
9. Monnin, E. et al. *Atmospheric CO_2 concentrations over the last glacial termination*. Science **291**, 112-114 (2001).
10. Joos, F. et al. *An efficient and accurate representation of complex oceanic and biospheric models of anthropogenic carbon uptake*. Tellus Series B-Chemical and Physical Meteorology **48**, 397-417 (1996).
11. Indermühle, A. et al. *Holocene carbon-cycle dynamics based on CO_2 trapped in ice at Taylor Dome, Antarctica*. Nature **398**, 121-126 (1999).
12. Joos, F., Gerber, S., Prentice, I. C., Otto-Bliesner, B. L. & Valdes, P. J. *Transient simulations of Holocene atmospheric carbon dioxide and terrestrial carbon since the Last Glacial Maximum*. Global Biogeochemical Cycles **18**, 1-18 (2004).
13. Mook, W. G. *^{13}C in Atmospheric CO_2*. Netherlands Journal of Sea Research **20**, 211-223 (1986).
14. Joos, F. & Bruno, M. *Long-term variability of the terrestrial and oceanic carbon sinks and the budgets of the carbon isotopes ^{13}C and ^{14}C*. Global Biogeochemical Cycles **12**, 277-295 (1998).
15. Bruno, M. & Joos, F. *Terrestrial carbon storage during the past 200 years: A Monte Carlo analysis of CO_2 data from ice core and atmospheric measurements*. Global Biogeochemical Cycles **11**, 111-124 (1997).
16. Prentice, I. C., Jolly, D. & participants, B. *Mid-Holocene and glacial-maximum vegetation geography of the northern continents and Africa*. J. Biogeogr **27**, 507–519 (2000).

Tables:

	$\delta^{13}C_{min}$ (‰)	$\delta^{13}C_{max}$ (‰)	T_{max} (‰)	$\delta^{13}C_{end}$ (‰)	(11-T_{max}) kyr BP increase (‰)	(T_{max}-T_{end}) kyr BP decrease (‰)
(1) uncorrected	-6.07	-5.83	6116	-5.89	0.24	-0.06
(2) corrected	-6.58	-6.33	5535	-6.38	0.25	-0.05

ST1: Summary of the main features of the spline through the uncorrected data set (1) and through the gravitation corrected data set (2). T_{max} is the year BP where the spline through the data reaches its maximum $\delta^{13}C$ value whereas $\delta^{13}C_{end}$ refers to the value of the spline for the most recent sample.

	$\delta^{13}C_{min}$ (‰)	$\delta^{13}C_{max}$ (‰)	T_{max} (‰)	$\delta^{13}C_{end}$ (‰)	11-8 kyr BP increase (‰/kyr)	6-0 kyr BP decrease (‰/kyr)
(1) cracker	-6.60	-6.32	5750	-6.35	-0.06±0.02	0.01±0.01
(2) sublimation	-6.64	-6.32	4800	-6.43	-0.07±0.03	0.018±0.009

ST2: Summary of the main features of the spline through the cracker data record (1) and through the sublimation data record (2) as well as the comparison between the linear slopes through the individual records and their uncertainties for the intervals 11-8 kyr BP and 6-0 kyr BP. T_{max} is the year BP where the spline reaches its $\delta^{13}C$ maximum whereas $\delta^{13}C_{end}$ refers to the value of the spline for the most recent sample.

Figures:

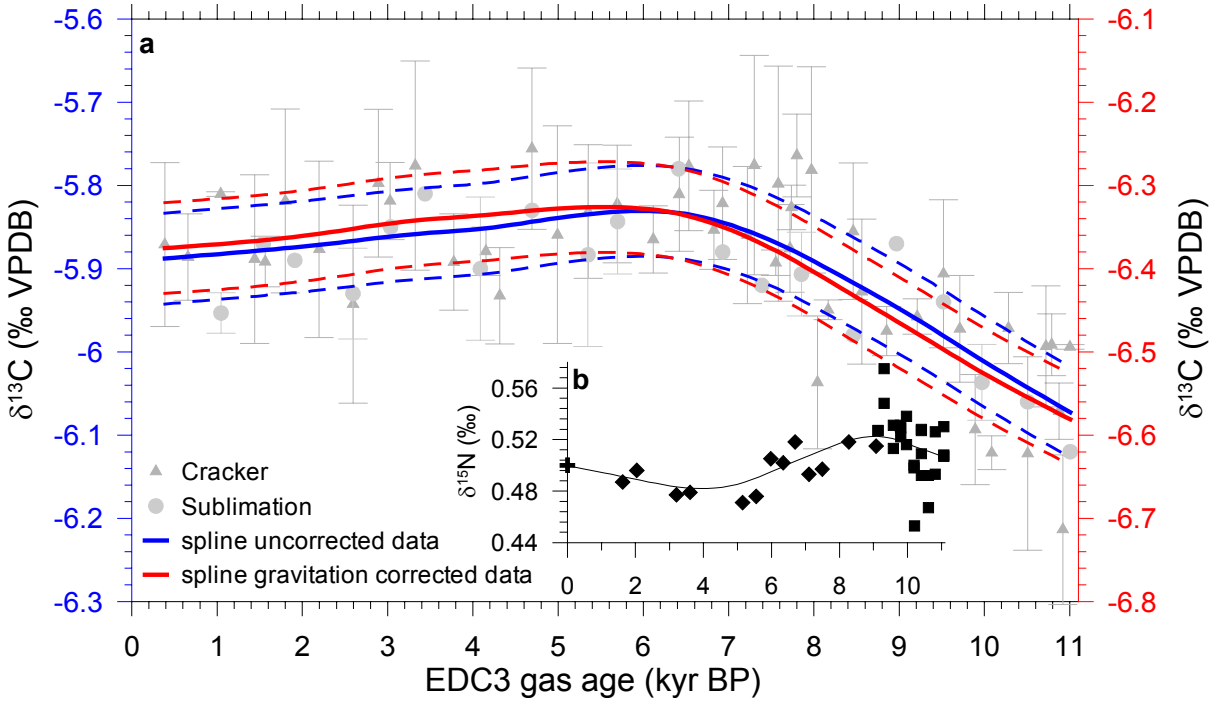

Figure S1: The effect of the gravitation correction on the $\delta^{13}C$ record. (a) The blue line is the spline through the uncorrected data set (left y-axis) with its 1σ uncertainty band (dashed line), whereas the red line corresponds to the spline through the gravitation corrected data set (right y-axis) with its corresponding 1σ band. (b) The inset corresponds to $\delta^{15}N$ data. The single $\delta^{15}N$ value at 0 yrs BP is taken from firn measurements (black cross)[3]. $\delta^{15}N$ values from 1 to 9 kyr BP are unpublished values measured at LSCE by D. Rodriguez, E. Capron and A. Landais in 2008 (black diamonds), and $\delta^{15}N$ values after 9 kyr BP were measured at LSCE by G. Dreyfus in 2003 (black squares). A spline through the $\delta^{15}N$ data was used to correct the $\delta^{13}C$ data. This spline indicates a mean correction of (0.50 ± 0.01)‰. Within the error band, the two splines through the $\delta^{13}C$ data agree. Therefore, the main conclusions of this paper are not affected by the gravitation correction.

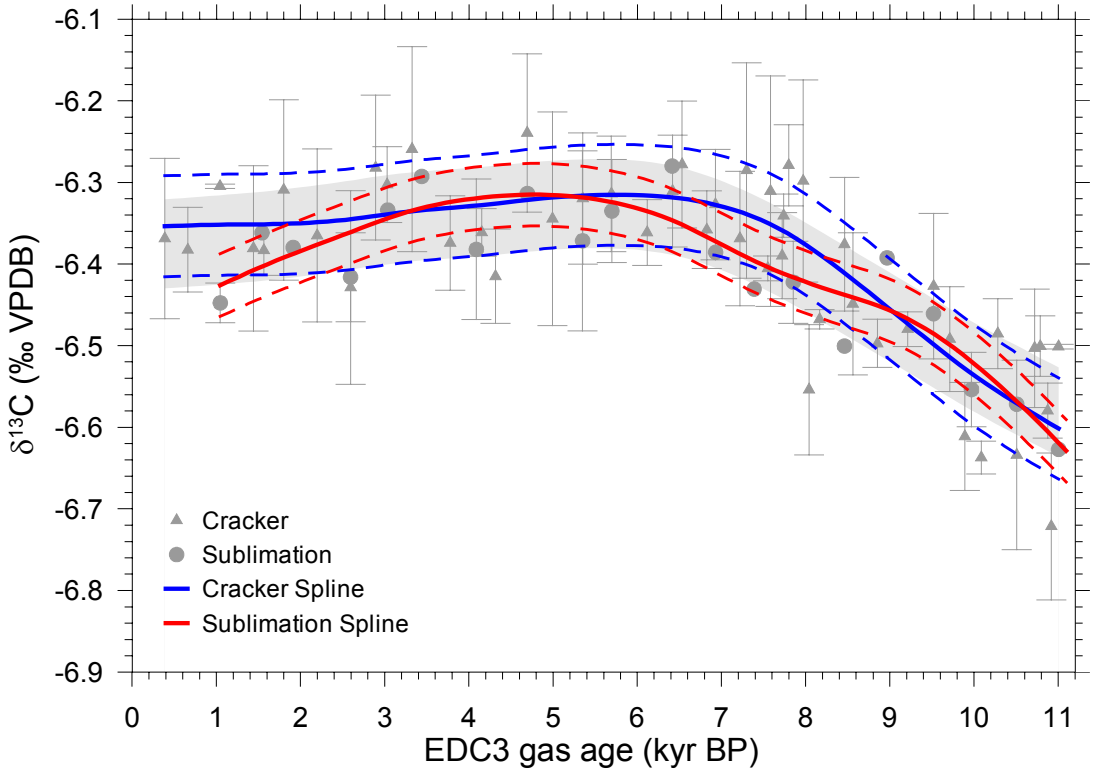

Figure S2: Spline through the cracker data set (blue line) with 1σ error band and the spline through the sublimation data set (red line). The grey shaded area is the 1σ band of the spline through both data sets. The two splines agree within their uncertainties. Therefore, an offset of the methods can be excluded.

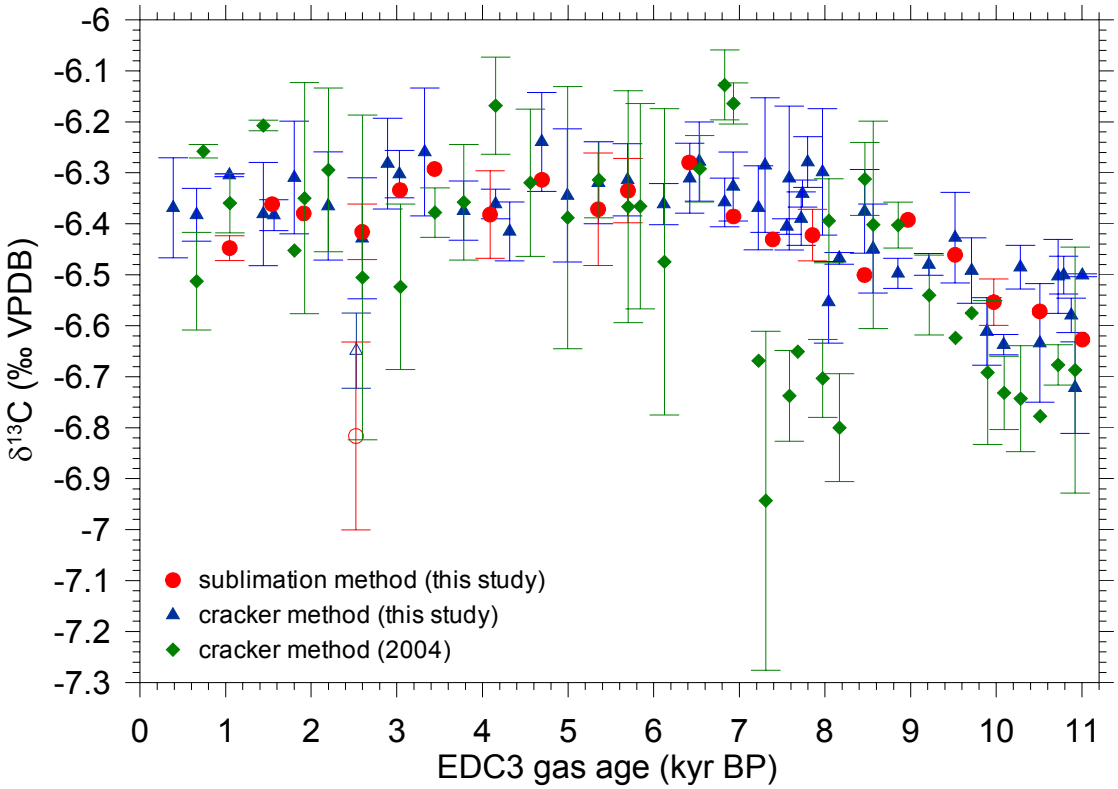

Figure S3: Comparison of the $\delta^{13}C$ data from this study with unpublished data (green diamonds, mean of mostly two samples, error bars are 1σ of the mean) established in 2004 in Bern[5] with a preliminary cracker method compared to the one used in this study.

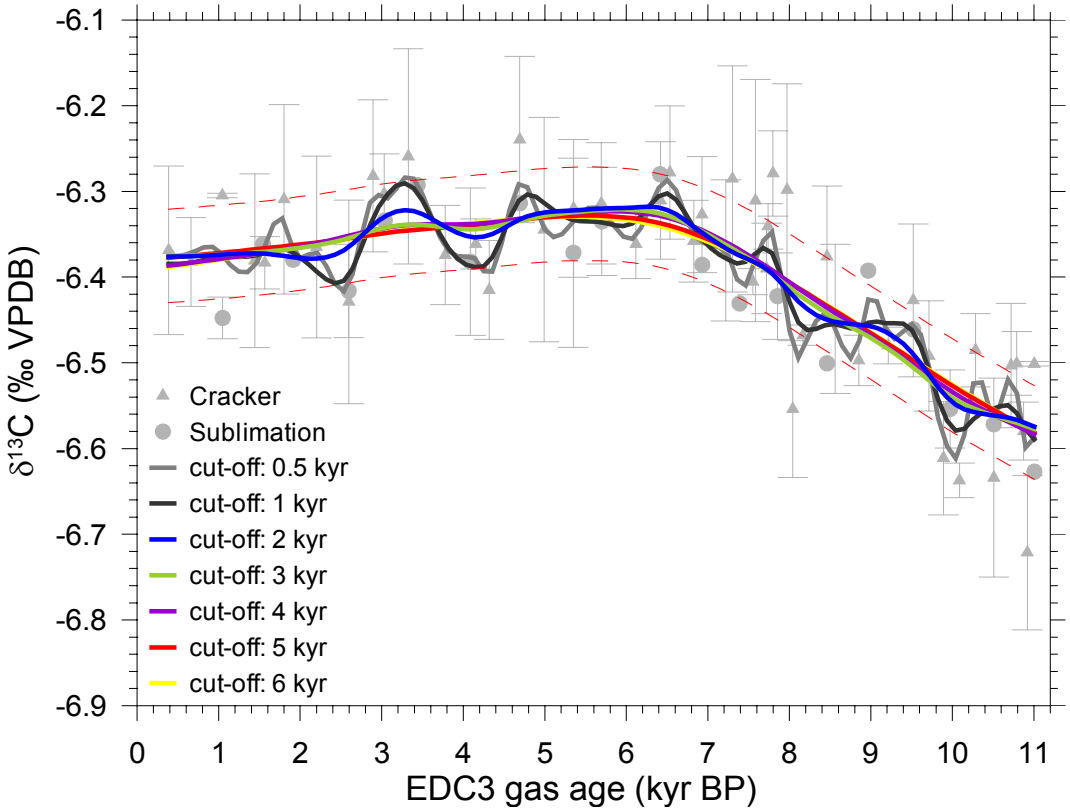

Figure S4: Splines of Monte-Carlo simulations with different cut-off periods. For cut-off periods longer than about 3 kyr, the oscillating behaviour of the splines disappears and the long-term trend becomes robust. The dashed red lines indicate the 1σ band of the spline with a cut off period of 5 kyr.

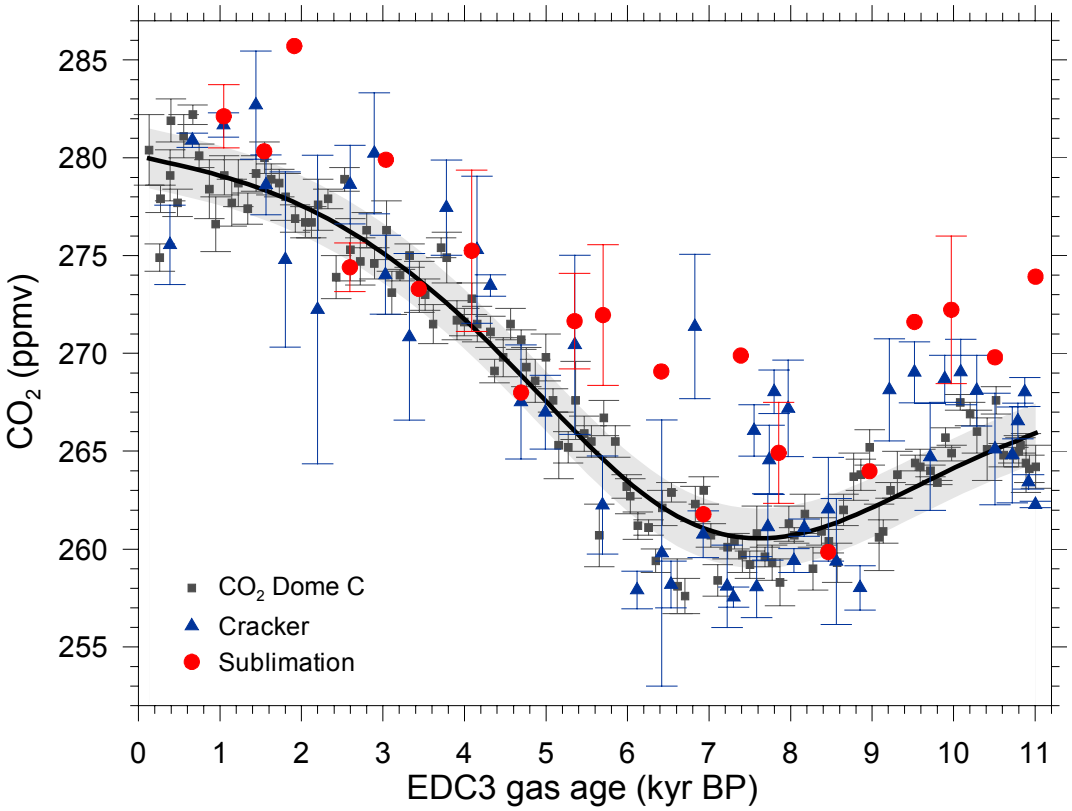

Figure S5: CO_2 record of air trapped in Dome C ice. Blue triangles are the measurements performed with the cracker set-up. Red circles are CO_2 concentration measurements obtained using the sublimation set-up. The error bars represent the t-weighted 1σ standard deviation of the mean. Grey squares are the CO_2 measurements from Monnin et al.[9]. The black line is the spline through the record of Monnin et al. with a cut-off period of 5 kyr and the grey shaded area is the corresponding 1σ band.

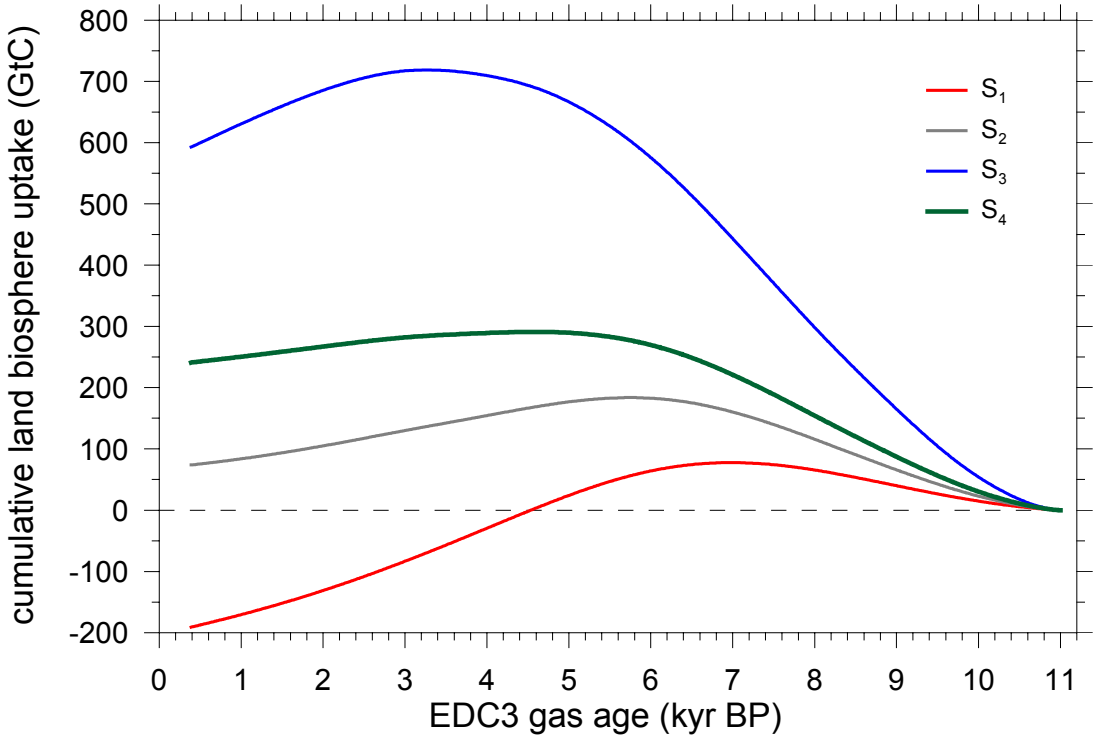

Figure S6: Cumulative land biosphere uptake from inverse modelling results for the discussed scenarios: (S_1: land-biosphere-only scenario, S_2: land biosphere-global SST scenario, S_3: land biosphere-marine biota scenario, S_4: land biosphere-marine carbonate compensation scenario).

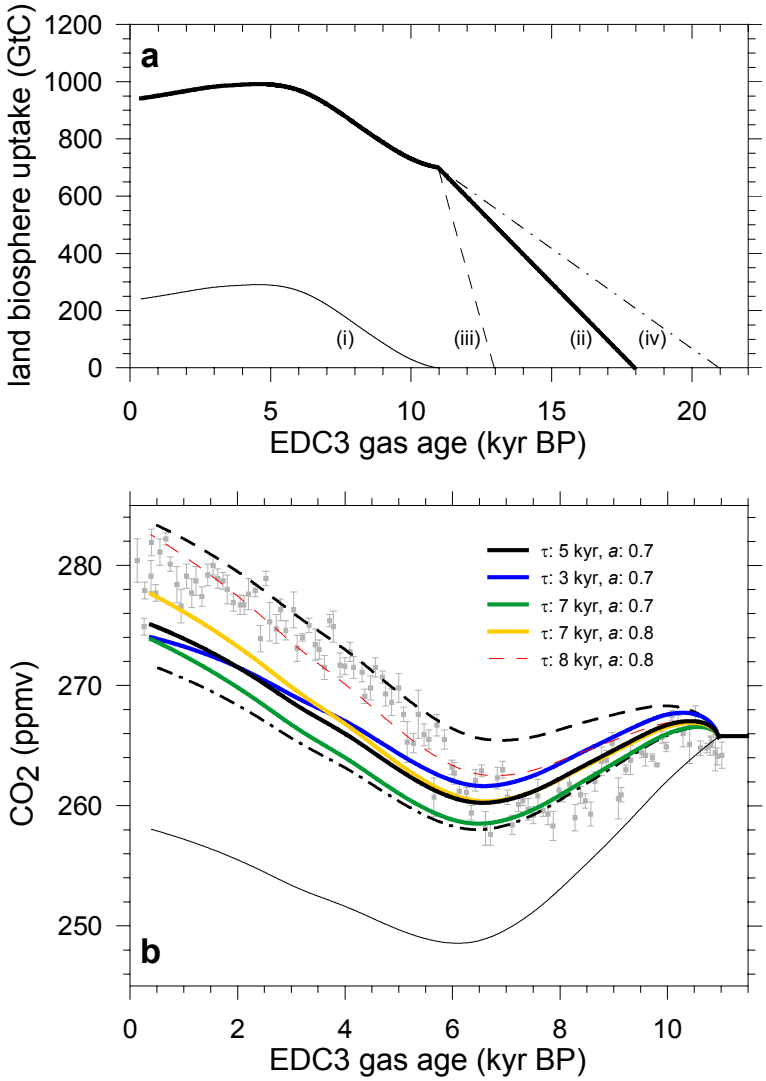

Figure S7: Sensitivity tests for the CO_2 evolution predicted by the land biosphere-marine carbonate compensation scenario S_4 during the Holocene. a) During the Transition, the cumulative land biosphere uptake of 700 GtC is prescribed by a linear increase in 7 kyr (thick black line, (ii)), in 2 kyr (dashed black line, (iii)) or in 10 kyr (dash-dotted black line, (iv)). After 11 kyr BP, the land biosphere uptake is dictated by the output of S_4. The black thin line shows the case where no terrestrial uptake took place over the Transition (i). b) The line character is given by the different uptake histories presented left whereas the colour describes the influence of changing τ and a.